BIOCHEMISTRY
including biophysical chemistry & molecular biology

Article

pubs.acs.org/biochemistry

Analysis of the Structural and Functional Roles of Coupling Helices in the ATP-Binding Cassette Transporter MsbA through Enzyme Assays and Molecular Dynamics Simulations

Tadaomi Furuta,[†] Tomohiro Yamaguchi,[‡] Hiroaki Kato,[‡] and Minoru Sakurai*[,†]

[†]Center for Biological Resources and Informatics, Tokyo Institute of Technology, B-62 4259 Nagatsuta-cho, Midori-ku, Yokohama 226-8501, Japan

[‡]Graduate School of Pharmaceutical Sciences, Kyoto University, 46-29 Yoshida-Shimo-Adachi-cho, Sakyo-ku, Kyoto 606-8501, Japan

Supporting Information

ABSTRACT: ATP-binding cassette (ABC) transporters are constructed from some common structural units: the highly conserved nucleotide-binding domains (NBDs), which work as a nucleotide-dependent engine for driving substrate transport, the diverse transmembrane domains (TMDs), which create the translocation pathway, and the coupling helices (CHs), which are located at the NBD−TMD interface. Although the CHs are believed to be essential for NBD−TMD communication, their roles remain unclear. In this study, we performed enzyme assays and molecular dynamics (MD) simulations of the ABC transporter MsbA and two MsbA mutants in which the amino acid residues of one of the CHs were mutated to alanines: (i) wild type (Wt), (ii) CH1 mutant (Mt1), and (iii) CH2 mutant (Mt2). The experiments show that the CH2 mutation decreases the ATPase activity (k_{cat}) compared with that of the Wt (a decrease of 32%), and a nearly equal degree of decrease in the ATP binding affinity (K_m) was observed for both Mt1 and Mt2. The MD simulations successfully accounted for several structural and dynamical origins for these experimental observations. In addition, on the basis of collective motion and morphing analyses, we propose that the reverse-rotational motions and noddinglike motions between the NBDs and TMDs are indispensable for the conformational transition between the inward- and outward-facing conformations. In particular, CH2 is significantly important for the occurrence of the noddinglike motion. These findings provide important insights into the structure−function relationship of ABC transporters.

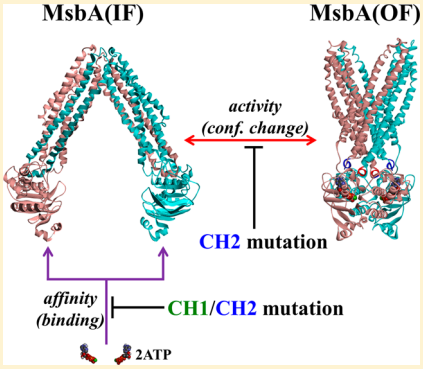

ATP-binding cassette (ABC) proteins constitute one of the largest superfamilies of integral membrane proteins found in all three domains of life (bacteria, archaea, and eukarya).[1−3] These ABC proteins are divided into main three classes: class 1 exporters, class 2 nontransport ABCs, and class 3 importers.[4] We focus mainly on ABC exporters (class 1), which, for the sake of simplicity, are called ABC transporters here. Canonical ABC transporters share a common structural organization comprising two nucleotide-binding domains (NBDs) that bind and hydrolyze ATP in the cytoplasm and two transmembrane domains [TMDs, also called membrane-spanning domains (MSDs)] that form the translocation pathway of substrates (see Figure 1A). Depending on the chemical and structural properties of TMDs, very diverse substrates are transported by ABC transporters, e.g., lipids, peptides, ions, and drugs.[2,5] In particular, with respect to drug transport, multidrug resistance (MDR) has recently become one of the most critical problems in medicine and molecular biology.[6−8]

The canonical NBDs of ABC transporters have seven conserved motifs, namely, Walker A (P-loop) and Walker B motifs,[9] ABC signature motif (or C-loop),[10] and the A-loop,[11] D-loop,[12] H-loop (switch motif),[13,14] and Q-loop,[15] on one ATP-binding pocket [ABP (Figure S1 of the Supporting Information)]; "canonical NBDs" refers to NBDs with two canonical (hydrolyzable) ABPs, and "noncanonical NBDs" refers to NBDs with one noncanonical (nonhydrolyzable) ABP and one canonical ABP. Five motifs, namely, the Walker A and B motifs and the A-, H-, and Q-loops, on one side constitute a half-pocket, whereas two motifs, namely, the ABC signature motif and the D-loop, make another half-pocket on the other side. Each of two ATP molecules is sandwiched between these half-pockets, mainly between the Walker A and ABC signature motifs in the outward-facing, NBD-dimerized conformation (Figure 1B). NBDs are dimerized in a head-to-tail manner such that there are two ABPs in an NBD dimer.[13,14,16,17]

The TMDs of ABC transporters (exporters) consist of 12 transmembrane helices (TMs), and each TMD has six TMs connected via intracellular and extracellular loops (ICLs and ECLs, respectively). From a structural point of view, these TMs make two wings depending on the conformations: TM1 and TM2 of one TMD and TM3−TM6 of the other TMD make up each wing in the outward-facing conformation [see Figure 1A; the left wing consists of TM1 and TM2 of TMD[B] (cyan) and

Received: February 28, 2014
Revised: June 2, 2014
Published: June 17, 2014

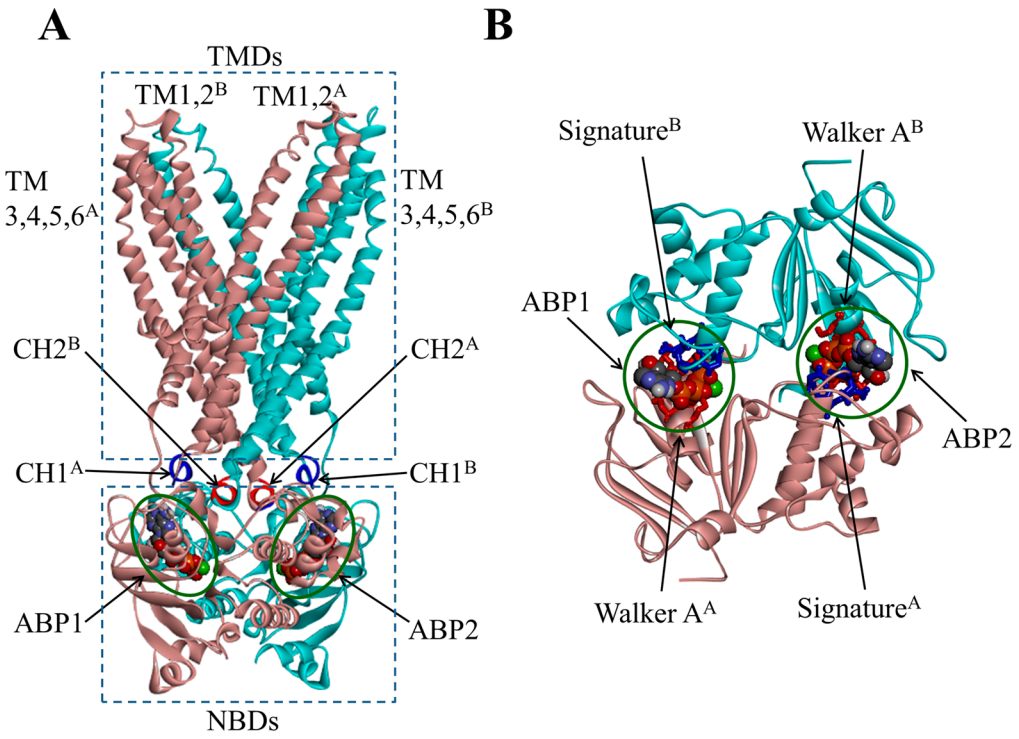

Figure 1. Structures of MsbA in an outward-facing conformation and its NBD dimer. (A) MsbA with two ATP molecules located in the ATP-binding pockets (ABP1 and ABP2). Each subunit is represented by ribbon models (subunits A and B are colored pink and cyan, respectively), and the TMD (top) and NBD (bottom) regions are enclosed by dashed boxes. The CH1s (blue), CH2s (red), and bound ATPs are denoted with arrows. (B) NBD dimer with two ATP molecules. The Walker A and signature motifs in each subunit are represented as red and blue sticks, respectively. The ATP molecules are represented by the CPK model. ABP1 and ABP2 are denoted with green circles in each panel.

TMD3 and TM4−TM6 of TMD^A (pink), and vice versa]. In the inward-facing conformation, TM1−TM3 and TM6 of one TMD and TM4 and TM5 of another TMD make up each wing. These wing-forming conformational changes between the inward- and outward-facing conformations are related to the ATP binding and/or hydrolysis at NBDs and substrate transport. Each TMD has two ICLs and three ECLs in the following order: TM1−ECL1−TM2−ICL1−TM3−ECL2−TM4−ICL2−TM5−ECL3−TM6. In particular, the NBD-interacting parts of ICLs are called coupling helices (CHs) (CH1 and CH2, shown in Figure 1A).[18]

The CHs are embedded in grooves on the surface of the NBD: CH1s in the grooves of the RecA-like core subdomain (CSD) and CH2s in the grooves at the boundary of the RecA-like core and the α-helical subdomains (HSDs) (see Figure S2 of the Supporting Information). In the NBD dimerized state, CH1s are positioned at the NBD−NBD interface, and thereby, each CH1 interacts with the HSD of the other NBD. In the representative ABC transporters Sav1866[18,19] and MsbA,[20] the CH2s are domain-swapped; that is, CH2 from subunit B interacts with the NBD of subunit A and vice versa, whereas each CH1 interacts with the same subunit NBD. Mutations at the transmission interface can cause transmission "uncoupling" or misassembly of ABC transporters.[21] The R378C (in CH2) mutant of human peptide transporter TAP1/2 yields a fully assembled transporter that hydrolyzes ATP; however, this mutant shows significant decreases in its levels of substrate binding and transport, and CH1 residue mutants interfere with the transport activity, suggesting that the ATP-driven conformational changes in the NBDs are not properly transmitted to the TMDs.[22] In the case of human CFTR, a deletion of F508 (located on the CH2-interacting interface in the NBD) is responsible for 66% of cystic fibrosis disease,[23] and this mutant exhibits fold defects that lead to premature degradation.[24,25] Similarly, in the case of human P-glycoprotein, a mutation of the phenylalanine residue (F1086), e.g., F1086A, is known to exert an unfavorable influence on the maturation and ATPase activity of the protein.[26] Several computational studies of ABC exporters (Sav1866[27−30] and ABCB1[29,31]) and an importer (MalFGK$_2$-E[32]) also suggested that the coupling helices are significant for the dynamic coupling of the full transporters. On the basis of these observations, the CHs are hypothesized to play an important role in the transmission of conformational changes at the NBDs to the TMDs via noncovalent interactions at the interfaces. However, the structural and functional roles of each CH remain unclear at the atomic level.

In this study, we selected MsbA as a model ABC transporter to examine the roles of the CHs because it has been extensively investigated from structural[20,33−36] and biochemical viewpoints.[37−43] To clarify the functional and structural roles of the CHs of MsbA, we performed enzyme assays and molecular dynamics (MD) simulations for wild-type MsbA and two mutants in which all of the amino acid residues constituting either CH1 or CH2 are mutated to alanines: (i) wild type (Wt), (ii) CH1 mutant (Mt1), and (iii) CH2 mutant (Mt2). Using the enzyme assays, we determined the kinetic parameters underlying the ATPase activity of each protein. We also conducted MD simulations for each protein and analyzed the structure and dynamics of the TMDs, NBDs, and ATP-binding pockets. Combining these results, we discuss the role of CHs.

dx.doi.org/10.1021/bi500255j | *Biochemistry* 2014, 53, 4261−4272

MATERIALS AND METHODS

Site-Directed Mutagenesis. The replacement of all amino acid residues on CH1 (V113SFFDKQ119) or CH2 (H214KEVL218) of *Escherichia coli* MsbA (EcMsbA) with alanines was performed using the QuikChange site-directed mutagenesis kit (Stratagene). The pET15b plasmid bearing the *EcMsbA* gene with an N-terminal hexahistidine affinity tag, which was reported previously,[33] was used as the template for the mutagenesis reactions. The forward and reverse primers for Mt1 are 5′-CATGATGGGAATGCCAGCTGCAGCCGCTGCCGCAGCGTCAACGGGTACG-3′ and 5′-GTACTACCCTTACGGTCGACGTCGGCGACGGCGTCGCAGTTGCCCATGC-3′, respectively. The forward and reverse primers for Mt2 are 5′-CAAATGCTGAAGGGCGCCGCAGCAGCAGCGATTTTCGGTGGTCAG-3′ and 5′-GTTTACGACTTCCCGCGGCGTCGTCGTCGCTAAAAGCCACCAGTC-3′, respectively.

Expression and Purification of MsbA. The expression and purification of MsbA were performed as described previously[33] with minor modifications. Briefly, the pET15b plasmid bearing the *EcMsbA* gene was transformed into *E. coli* strain C41(DE3). Protein expression was induced by the addition of 0.2 mM isopropyl β-D-1-thiogalactopyranoside at 37 °C for 4 h. All of the steps in the purification process, which are described below, were performed at 0−4 °C. The recovered cells were resuspended in 20 mM Tris-HCl (pH 8.0), 300 mM NaCl, 10 mM imidazole, and 1 mM PMSF, disrupted by sonication, and centrifuged to obtain the soluble fraction. The cell lysates were solubilized with 1% (w/v) *n*-dodecyl β-D-maltopyranoside (β-DDM) (Anatrace, Maumee, OH) and ultracentrifuged at 100000*g* for 45 min. The supernatant was applied to a Talon affinity resin (BD Biosciences, Palo Alto, CA) equilibrated with wash buffer [20 mM Tris-HCl (pH 8.0), 300 mM NaCl, 20 mM imidazole, and 0.03% (w/v) β-DDM]. The column was washed with 10 bed volumes of wash buffer, and EcMsbA was eluted with 20 mM Tris-HCl (pH 8.0), 300 mM NaCl, 300 mM imidazole, and 0.03% (w/v) β-DDM. The fractions containing EcMsbA were separated via gel filtration using a Superdex200 16/60 gel filtration column (GE Healthcare) with running buffer [20 mM Tris-HCl (pH 8.0), 150 mM NaCl, and 0.03% (w/v) β-DDM].

Enzyme Assays. The ATPase activities were measured by incubating the purified protein with 5 mM $MgCl_2$ and various concentrations of ATP in 40 mM Tris-HCl (pH 7.5), 0.03% (w/v) β-DDM, 0.1 mM EGTA, and 2 mM dithiothreitol at 37 °C. The ATPase reaction was initiated by mixing 20 μL of the protein solution with 180 μL of the ATP solution containing $MgCl_2$ and ATP at 37 °C; before being mixed, both of these solutions were preincubated separately at 37 °C for 5 min. The final protein concentrations were 1, 2, and 6 μg/mL for the Wt, Mt1, and Mt2, respectively. The final $MgCl_2$ concentration was 5 mM, and the final ATP concentration was 0−3 mM for the Wt and 0−3.5 mM for Mt1 and Mt2. At 0, 5, 10, 15, 20, and 25 min after the protein and ATP solutions had been mixed, 20 μL of the samples was mixed with 12% SDS to stop the reaction. The amount of released inorganic phosphate was measured using a colorimetric method.[44] The concentration of inorganic phosphate was plotted against the reaction period, and the initial ATP hydrolysis rate was calculated from the gradient of these plots. The kinetic parameters were determined using the Michaelis−Menten equation (eq 1):

$$v = \frac{k_{cat}[e][s]}{K_m + [s]} \quad (1)$$

where v is the initial ATP hydrolysis rate, [s] is the ATP concentration, [e] is the MsbA concentration, k_{cat} is the catalytic constant of ATPase activity, and K_m is the Michaelis constant. The fitting was performed through nonlinear regression using GRAFIT (version 5.04, Erithacus Software).

Preparation of MD Starting Structures. The atomic coordinates of *Salmonella typhimurium* MsbA were obtained from Protein Data Bank (PDB) entry 3B60 (chains A and B).[20] This structure takes an outward-facing conformation with two AMP-PNP molecules bound to the NBDs. These AMP-PNP molecules were replaced with two ATP molecules, and two Mg^{2+} ions were subsequently added in reference to the crystal structure of MJ0796 (PDB entry 1L2T).[13] The resultant structure was embedded into the optimal position of a 1-palmitoyl-2-oleoylphosphatidylcholine (POPC) lipid bilayer [quadruplicate of the 128-POPC bilayer downloaded from Tieleman's Web site (http://moose.bio.ucalgary.ca/)] based on the Orientations of Protein in Membranes (OPM) database.[45] The POPC molecules were rearranged to fit the TMDs using the "shrinking" method,[46] and a total of 504 POPC molecules remained after this process. This MsbA-plus-membrane system was solvated by water molecules, and those located in the intramembrane region were then removed manually. For the ATP-bound state, four Cl^- ions were added to preserve the electrostatic neutrality of the system, whereas six Cl^- ions were added for the apo state. This difference arises from the ATP-plus-Mg^{2+} charge and the protonation state of the H-loop histidines (residue 573 on each subunit): these are protonated in the ATP-bound state and nonprotonated in the apo state. The total numbers of atoms in the ATP-bound and apo systems were 253670 and 253583, respectively. For the mutants of Mt1 and Mt2, the side chains of residues 113−119 (VAFFDKQ) of CH1 and residues 214−218 (HKEVL) of CH2 were all mutated to alanines, and the corresponding number of Cl^- ions was added to ensure electrostatic neutrality. In this study, we prepared a total of six systems: Wt-ATP, Mt1-ATP, and Mt2-ATP in the ATP-bound states and Wt-apo, Mt1-apo, and Mt2-apo in the apo states.

MD Simulations. All of the MD simulations were performed using GROMACS version 4.0.7.[47] The GROMOS-87 force field with corrections was used for the proteins, ATP, and Cl^- ions,[48−50] and the SPC model was used for water.[51] In the original force field for ATP, the γ-phosphate is protonated (−3*e*), whereas it should be deprotonated under physiological conditions; i.e., the total charge of ATP is −4*e*. In this study, we modified the original ATP force field through deprotonation of the γ-phosphate and redistribution of the partial charges evenly over the phosphate oxygen atoms. For the POPC lipid, we used the modified Berger force field.[52,53] For each system, energy minimization was first performed until the maximal force was <10 kJ mol^{-1} $Å^{-2}$ with positional restraints of 10 kJ mol^{-1} $Å^{-2}$ on the heavy atoms of the proteins, ATP, and Mg^{2+} ions. The equilibration was then performed for 5 ns under *NPT* conditions (1 bar and 310 K) using the same positional restraints that were used for the minimization. The production run was performed under the same *NPT* condition for 100 ns without any restraints. In these MD processes, the Nosé−Hoover thermostat and the Parrinello−Rahman barostat were used for the temperature and pressure controls, respectively.[54−56] The electrostatic interactions were calculated

using the particle mesh Ewald (PME) method[57,58] with a cutoff distance of 1.2 nm, and the same cutoff was used for the van der Waals (vdW) interactions. The LINCS algorithm was used for all of the bond constraints of proteins and ATPs,[59,60] and SETTLE was used for the SPC water molecules[61] with a time step of 2 fs.

To confirm the reproducibility of several key results, especially for the collective motions of the protein, we performed two additional production runs for Mt1-ATP and Mt2-ATP systems for the initial relaxation phase (0−20 ns). Moreover, we performed three MD runs using the GROMOS43A1-S3 force field[62,63] to determine whether the key results obtained depend on the force field employed.

RESULTS

ATPase Activity. The effect of the mutations on the biochemical function of EcMsbA was assessed by measuring the ATPase activities of purified Wt, Mt1, and Mt2 in the presence of various concentration of ATP (Figure 2), and the kinetic

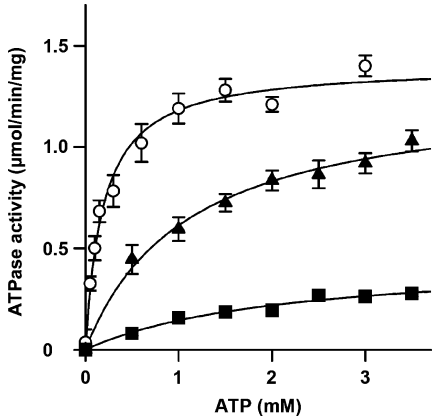

Figure 2. Kinetics of ATP hydrolysis by Wt, Mt1, and Mt2 MsbA. The ATPase activities of Wt (○), Mt1 (▲), and Mt2 (■) MsbA were measured at 37 °C in 40 mM Tris-HCl (pH 7.5), 0.03% (w/v) β-DDM, 0.1 mM EGTA, 2 mM dithiothreitol, and 5 mM $MgCl_2$ as a function of ATP concentration. All of the data points represent the means ± the standard deviation from two independent assays. The solid lines are fits of equations to the data using the Michaelis−Menten equation (Materials and Methods).

parameters (k_{cat} and K_m) are summarized in Table 1. As a result, there were no considerable differences in the values of the catalytic rate constant k_{cat} between Wt and Mt1: their k_{cat} values were 1.56 ± 0.05 and 1.43 ± 0.07 s^{-1}, respectively. In contrast, the k_{cat} value of Mt2 was decreased to 32% of that of the Wt (0.504 ± 0.063 s^{-1}). In contrast, the apparent affinity for ATP of both Mt1 and Mt2 was reduced compared with that of the Wt (the K_m values of Wt, Mt1, and Mt2 were 0.189 ± 0.024, 1.09 ± 0.15, and 2.14 ± 0.55 mM, respectively). These results suggest that the modification of CH2 affects the catalytic efficiency of EcMsbA more than that of CH1, whereas the CH1 or CH2 modification affects the affinity of the protein for ATP to the same extent.

Table 1. Kinetics of ATP Hydrolysis in Wt, Mt1, and Mt2 MsbA[a]

	k_{cat}[b] (s^{-1})	K_m[c] (mM)
Wt	1.56 ± 0.05	0.189 ± 0.024
Mt1	1.43 ± 0.07	1.09 ± 0.15
Mt2	0.504 ± 0.063	2.14 ± 0.55

[a]Kinetic parameters were determined using the Michaelis−Menten equation (Materials and Methods). Data are means ± the standard error. [b]k_{cat} is the catalytic constant of ATPase activity. [c]K_m is the Michaelis constant.

Structural Stability. The root-mean-square deviations (rmsds) of the Cα atoms from the initial structure were separately calculated for NBDs, TMDs, and the whole protein using the MD trajectories of the six systems studied (Wt-ATP, Mt1-ATP, Mt2-ATP, Wt-apo, Mt1-apo, and Mt2-apo). The results are shown in Figure 3 (NBDs and TMDs) and Figure S3 of the Supporting Information (whole protein). In all of the cases, the rmsd converged well to a constant value after approximately 40 ns. The final whole-protein rmsd value of the Wt-ATP system exhibited a value of 2.76 Å (<3 Å), which is lower than that (approximately 3.5 Å) obtained for the Wt-apo system (Figure S3 of the Supporting Information). As expected, the rmsd values of all of the mutant systems were >4 Å in the ATP-bound and apo systems.

With a focus on the NBDs (Figure 3A,B), the final rmsd values in the ATP-bound state are relatively small (<2.5 Å) and nearly equal among the three systems: Wt-ATP, Mt1-ATP, and Mt2-ATP. In the ATP-free (apo) state, however, the rmsd values were larger (>2.5 Å) than the corresponding values in the ATP-bound state. This finding implies that the ATP molecules accommodated in the ABPs act as a molecular glue on the NBD−NBD interface to stabilize their dimer structure.[17,64] Among the three apo systems (Figure 3B), Mt2-apo exhibited the largest change in its rmsd with a final value of 3.23 Å, suggesting that the CH2 mutation causes significant instability in the NBD structure. With a focus on the TMDs (Figure 3C,D), the CH2 mutations also induce large structural changes in the TMD regions in the ATP-bound and apo states; the final rmsd values for these states were 3.21 and 3.56 Å, respectively. However, the difference between the CH1 and CH2 mutants is not significant for the TMD regions.

Structural Changes in the Protein. As a measure of the structural changes of TMDs, we chose the distances between $Gly57^A$ and $Gly57^B$, which are located in the termini of ECL1s in the two wings (Figure 4). A change in this distance corresponds to the opening or closing of the two TMD wings. The initial distance of this Gly57 pair was approximately 33 Å. Over time, the MD shows that this distance decreases by 5.2 Å in the Mt2-ATP system, whereas relatively small increases were found in the Wt-ATP and Mt1-ATP systems (4.0 and 2.3 Å, respectively). In the apo state, a significant decrease in this distance was observed in all three systems studied, and the largest change (−7.3 Å) was found in Mt2-apo. Taken together, the data show that the CH2 mutation induces a closing of the TMD wings irrespective of whether ATP molecules are bound to the ABPs.

To quantify the structural change in the NBD, we measured the distance between the Walker A and ABC signature motifs, which are located in the ABPs to trap ATP molecules (see Figure 1B). In all of the ATP-bound states studied, this intermotif distance was maintained to be approximately 9 Å at both ABPs during the MD simulation (see Figure 5A−C), which indicates that each ATP molecule located in each APB is tightly grasped between the Walker A and signature motifs. Interestingly, in the Wt-apo and Mt1-apo systems, asymmetric changes were observed with respect to the two ABPs (see Figure 5D,E): substantial increases at the ABP1 site (1.3 and

dx.doi.org/10.1021/bi500255j | Biochemistry 2014, 53, 4261−4272

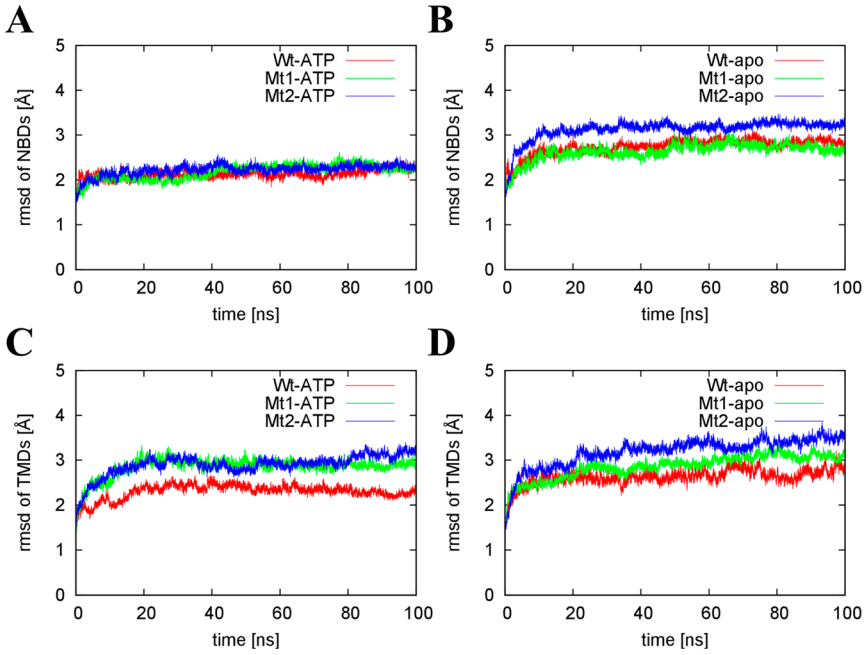

Figure 3. rmsds for the Cα atoms of NBDs and TMDs. (A) Data for the NBDs in the ATP-bound states. (B) Data for the NBDs in the apo states. (C) Data for the TMDs in the ATP-bound states. (D) Data for the TMDs in the apo states. In each figure, the data for the Wt, Mt1, and Mt2 are colored red, green, and blue, respectively.

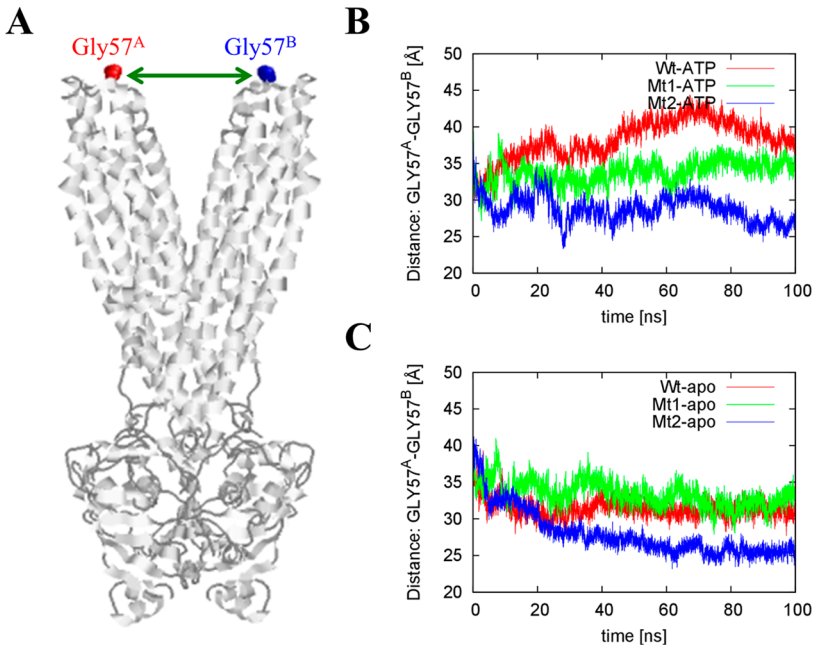

Figure 4. Interterminal distances on the extracellular side. (A) The positions of the extracellular terminal residues Gly57^{A} and Gly57^{B} in ECL1s are represented by red and blue spheres, respectively. The interterminal distance measured is indicated by the green double-headed arrow. (B and C) Interterminal distances for the ATP-bound and apo states, respectively. The data for Wt, Mt1, and Mt2 are colored red, green, and blue, respectively.

3.4 Å, respectively) and decreases at the ABP2 site (1.2 and 0.3 Å, respectively). In contrast, in the Mt2-apo system, the intermotif distance of interest decreased in both of the ABPs (0.2 Å for ABP1 and 1.4 Å for ABP2) (see Figure 5F), indicating the uniqueness of Mt2 in terms of dynamics compared with Wt and Mt1.

If we pay attention to the Wt-apo system, the degree of asymmetry between the two ABPs begins to increase at approximately 30 ns and reached a plateau with a value of approximately 2.5 Å near 40 ns (Figure 5D). In contrast, in the TMD region, the change in the interwing distance steeply decreased up to 30 ns and reached the plateau after approximately 40 ns (Figure 4C). The interwing distance of TMDs was also measured between Met276^{A} and Met276^{B}, which are located at the ECL3s of each subunit. The results confirmed that this distance starts to markedly fluctuate after 40 ns [see Wt-apo (red) in Figure S4D of the Supporting Information]. Therefore, it can safely be concluded that some local domain motions, the asymmetric motion between the two NBDs, and the closing and/or opening of the TMD wings

dx.doi.org/10.1021/bi500255j | *Biochemistry* 2014, 53, 4261−4272

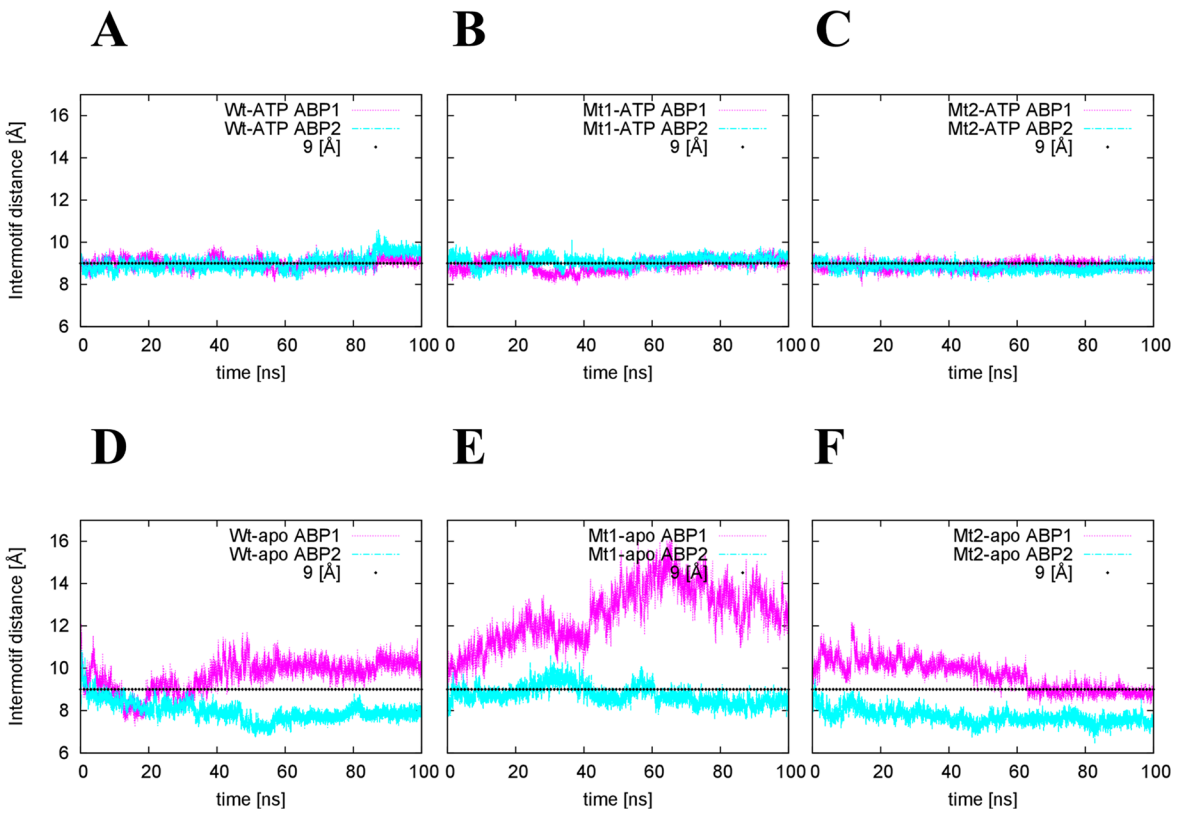

Figure 5. Intermotif distances between Walker A and signature motifs in ABP1 (magenta) and ABP2 (cyan) for (A) Wt-ATP, (B) Mt1-ATP, (C) Mt2-ATP, (D) Wt-apo, (E) Mt1-apo, and (F) Mt2-apo.

occur in a synchronous fashion. The occurrence of such synchronized motions in the apo state implies that the protein structure changes toward an inward-facing conformation after ATP hydrolysis, consistent with previous reports.[28,29,65,66]

Structure of the ATP-Binding Sites. Because CH1 is located near the adenine part of ATP, the CH1 mutation is hypothesized to affect the A-loop, which directly interacts with the adenine part of ATP in a hydrophobic manner ($\pi-\pi$ interaction). The distances between each A-loop (Try351) and the adenine moiety in the three ATP-bound systems are shown in Figure 6B–D. In the Mt1-ATP system (Figure 6C), the distance gradually increased until it reached 8.62 Å at ABP1. The initial and final positions of Try351 and ATP at ABP1 are depicted in Figure 6A, and the final structure shown demonstrates that Try351 is considerably distant from the adenine moiety of ATP. This finding suggests that the CH1 mutation likely significantly affects the affinity for ATP.

To examine the interaction between the phosphate group of ATP and its surrounding residues, we measured the distances between His537 on each H-loop and the Pγ atom of ATP (see Figure S5 of the Supporting Information). Each H-loop histidine was protonated in the ATP-bound state and thereby has a strong electrostatic attraction with the Pγ atom of ATP. In the Wt-ATP and Mt1-ATP systems, this distance is maintained at approximately 6.5 Å throughout the MD simulation (Figure S5B,C of the Supporting Information; the final structure for Wt-ATP is depicted in Figure S5A of the Supporting Information). In contrast, a small but distinct increase (>1.5 Å) with a large fluctuation in the H-loop was observed in ABP1 of the Mt2-ATP system (Figure S5D of the Supporting Information). This finding suggests that the electrostatic attraction of the H-loop with ATP is weakened by the CH2 mutation.

Collective Motions. We conducted principal component analysis (PCA) for the initial relaxation phases (0–20 ns) of the MD trajectories in the ATP-bound state. To pick up principal components that significantly contribute to the global motion of the protein of interest, we examined the percentage contribution of each PC (Figure S6 of the Supporting Information). The contributions of the first, second, and third PCs were as follows: 47.3% for first, 13.6% for second, and 4.3% for third in Mt1-ATP, 48.0% for first, 7.9% for second, and 5.1% for third in Mt2-ATP, and 27.7% for first, 13.4% for second, and 8.2% for third in Wt-ATP. Interestingly, the percentage contribution steeply decreases on going from the first to the second mode in the Mt1-ATP and Mt2-ATP systems. Thus, as a first approximation, we focus only on the first PC for comparison of their motional characteristics. In the Wt-ATP system (Figure 7A), the eigenvector of the first PC was identified as local atomic displacements around the NBDs accompanied by small swinging motions of TMDs. Thus, the Wt-ATP system did not exhibit any large collective motion over the whole protein. In contrast, a characteristic global motion was observed for the first PC mode of both mutant systems: NBD and TMD both rotate about the *y*-axis (molecular axis) in the opposite way with respect to each other (Figure 7B,C). Hereafter, we call this resultant motion "reverse-rotational" motion. It is noteworthy that the direction of rotation was opposite between the Mt1-ATP and Mt2-ATP systems: the first PC modes in the Mt1-ATP and Mt2-ATP systems correspond to clockwise (CW) and anticlockwise (ACW) rotations, respectively (Figure 7B,C). These reverse-rotational motions were also observed in two other independent MD runs using

dx.doi.org/10.1021/bi500255j | *Biochemistry* 2014, 53, 4261–4272

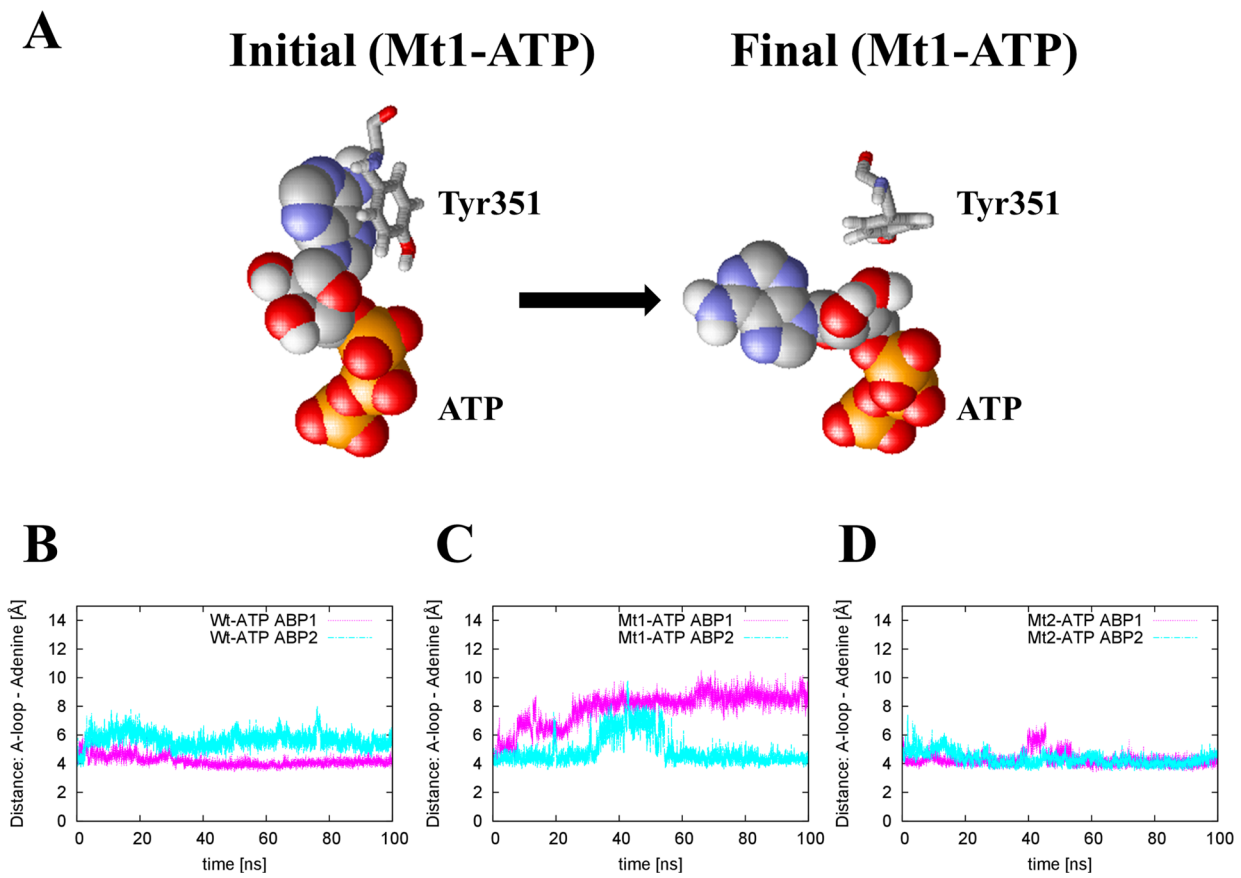

Figure 6. Interactions of ATP with the A-loop in the ATP-bound state. (A) Initial and final snapshots of Ty351 (stick) on the A-loop and ATP (sphere) at ABP1 in the Mt1-ATP system. (B) The distances between Tyr351 and the adenosine part of ATP for the Wt-ATP system are plotted, and the distances on ABP1 and ABP2 are colored magenta and cyan, respectively. (C and D) Corresponding distances for the Mt1-ATP and Mt2-ATP systems, respectively, are plotted in the same manner.

the same force field (GROMOS-87 with corrections) (left three columns, Figure S7 of the Supporting Information), and in three runs that were performed using the GROMOS43A1-S3 force field (right three columns, Figure S7 of the Supporting Information). These observations for the initial relaxation phase indicate that the mutation of either CH drastically changes the dynamics of the whole protein because of a characteristic collective motion, such as reverse-rotational motion. In other words, the results indicate that the CHs are essential for the maintenance of the native three-dimensional (3D) arrangement between the NBDs and TMDs.

The interdomain interactions among the CHs, the TMD wings, and the NBDs on one side are depicted in Figure 7D. In the wild-type protein, CH1 interacts with a RecA-like CSD, whereas CH2 is located between the CSD and HSD (these interactions are represented by the green and blue arrows, respectively, in Figure 7D). The replacement of the residues in each CH with alanines, which decreases the volume of the side chain, could collapse the space between each CH and the interacting region of the NBD. Therefore, the different interactions of CH1 and CH2 with NBDs are likely to cause the opposite reverse rotations observed in the Mt1-ATP and Mt2-ATP systems mentioned above. Table S1B of the Supporting Information lists the residues responsible for the CH−NBD or CH−CH interactions in the ATP-bound state. As described above, CH1 interacts with the CSD (Y351, F392, and Y393) and CH2 interacts with the CSD (F392, R416, and S423) and the HSD (V426, H427, F429, and R493) simultaneously (Table S1B of the Supporting Information). CH1 also interacts with the HSD of the opposite side NBD (E476, V479, and L480) in the NBD dimer state, probably leading to the stabilization of the NBD dimer structure. Furthermore, the direct interaction between F116 of CH1 and H214 of CH2 was observed in all the systems. It should also be noted that the total number of these interacting residues in the Mt2-ATP system is considerably smaller than those for the Wt-ATP and Mt1-ATP systems (Table S1A of the Supporting Information), which implies that the NBD−TMD communication is disturbed in the CH2 mutant.

For the apo state, we also conducted PCA for the whole period (0−100 ns) of the MD simulation (Figure S8 of the Supporting Information). In PC1, the asymmetric motions for the NBDs mentioned above were observed for the Wt-apo and Mt1-apo systems (see Figure S8A,B of the Supporting Information). In contrast, the Mt2-APT system exhibited motions that caused shrinkage of the ABPs (Figure S8C of the Supporting Information). The contributions of this mode reached 50%, which indicates that they dominate the overall motion of the protein. For the TMD, a wing-closing motion was observed in the Wt-apo system (see Figure S8D of the Supporting Information).

DISCUSSION

Relationship between ATPase Activity and CH Mutations. To reveal the functional role of the coupling helices (CH1 and CH2), we first performed enzyme assays for

dx.doi.org/10.1021/bi500255j | *Biochemistry* 2014, 53, 4261−4272

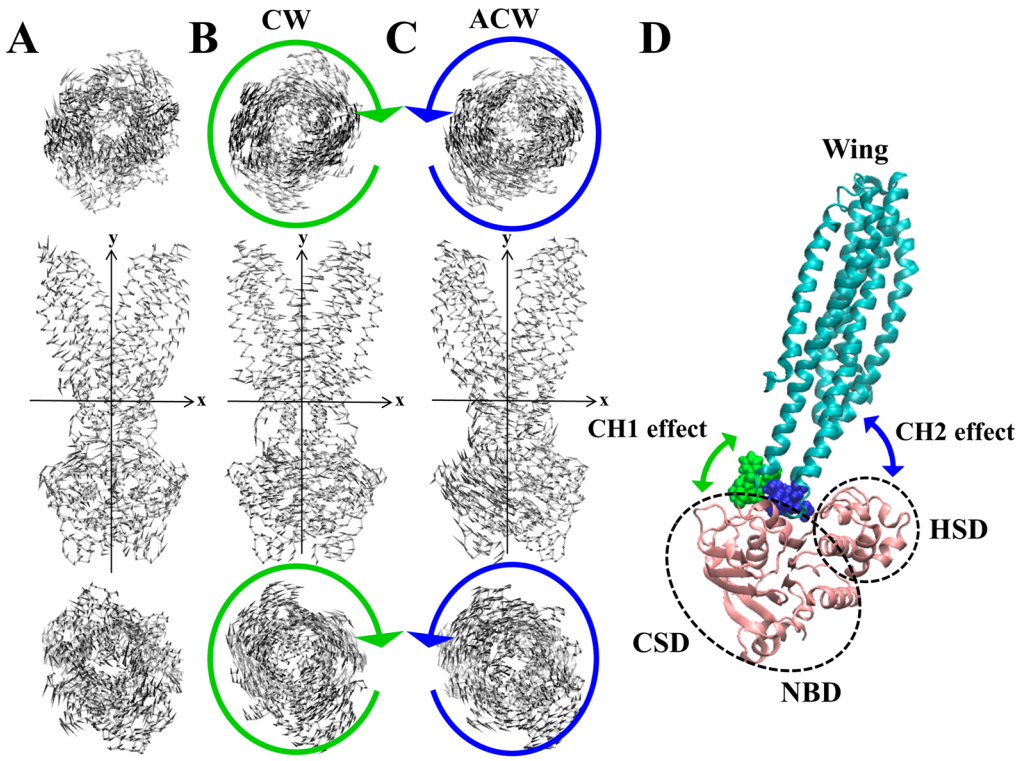

Figure 7. First PC eigenvectors of the initial phases in the ATP-bound state and effects of CH1 and CH2 on half of the NBD−TMD assembly (the whole protein). The top, side, and bottom views of the first PC eigenvector in (A) Wt-ATP, (B) Mt1-ATP, and (C) Mt2-ATP are shown. The reverse-rotational motions described in the text are represented by rotational arrows (green and blue for Mt1-ATP and Mt2-ATP, respectively). The eigenvectors in these three systems are represented by the thin black arrows. (d) The effects of CH1 and CH2 on half of the NBD−TMD assembly are depicted by double-headed arrows (green and blue, respectively). The CH1 and CH2 residues are represented by green and blue spheres, respectively. The NBD and TMD wing are represented as pink and cyan ribbons, respectively. The CSD and HSD are represented by dotted circles.

the ABC transporter MsbA (Wt) and two mutants, namely, Mt1 and Mt2. The experimental results show that the mutation of CH2 (corresponding to Mt2) decreases the ATPase activity (k_{cat}) to 32% of that of Wt, and significant reductions in the ATP binding affinities (K_m) were observed for both Mt1 and Mt2. To gain insight into the mechanism underlying these observations, we performed MD simulations.

We first discuss the change in affinity for ATP (and Mg^{2+} ion) due to the mutations. In ABC transporters, ATP is considered to bind to NBD through mainly two types of attractive interactions. The first is a $\pi-\pi$ stacking interaction between the adenine part of ATP and its nearby aromatic residue (A-loop[11]). The second interaction is an electrostatic interaction between the negative charges of the γ-phosphate groups of ATP and its nearby positively charged residue(s) (Walker A motif[9] and H-loop[13,14]) and between the positive charges of the Mg^{2+} ion and its nearby negatively charged residue(s) (Q-loop[15] and Walker B motif[9]). In the case of MsbA, the aromatic residue in the vicinity of the ATP adenine ring is Tyr351, which is located on the A-loop. As shown in the initial structure of the MD simulation, these residues are stacked on each other (Figure 6A, left). As observed for Mt1 (Figure 6A,C, right), this stacking was disrupted by the CH1 mutation. In contrast, the electrostatic interaction between the γ-phosphate of ATP and His537 located in the H-loop was found to be weakened by the CH2 mutation, which can be observed from the increase in their inter-residue distance by approximately 1.5 Å with a relatively large fluctuation at the Pγ site of ABP1 (Figure S5D of the Supporting Information). In our simulations, the events induced by the CH mutations were observed at either of the two ABPs. However, considering their stochastic nature and the structural equivalence of the two ABPs, we can safely state that similar events would occur at the alternative APB site if we conducted longer MD runs or a larger number of MD runs. Taken together, the data demonstrate that the affinity for ATP is reduced by mutations of the CH moieties.

In the Q-loop of the ABC transporter, there is a conserved glutamine residue, which interacts with Mg^{2+} and an oxygen atom of hydrolyzable water.[13] In addition, some of the upstream and downstream residues of the Q-loop interact with CH2.[3,18,67] These interactions were also found in our MD simulations (Table S1 of the Supporting Information). Thus, it is expected that the ATPase activity is influenced by the CH2 modification through the Q-loop. However, in the X-ray structure of MsbA used in this study (PDB entry 3B60), the corresponding conserved glutamine residue, Gln424, in the Q-loop is flipped in both ABPs (Figure S1 of the Supporting Information) and does not directly interact with the Mg^{2+} ion or a hydrolyzable water molecule around the γ-phosphate of ATP. Such an unfavorable situation was maintained throughout the MD simulation for each of the ATP-bound systems. Consequently, we are unable to discuss the effect of the CH mutation via the Q-loop on enzymatic activity (k_{cat}).

Another important residue that likely contributes to ATPase activity is a conserved histidine in the H-loop,[17,68] namely His357 in the case of MsbA. This type of histidine functions as a "linchpin" that holds together the γ-phosphate of ATP, the attacking water (hydrolyzable water), and the catalytic base (glutamic acid, Glu506) for catalysis. The substitution of this

dx.doi.org/10.1021/bi500255j | *Biochemistry* 2014, 53, 4261−4272

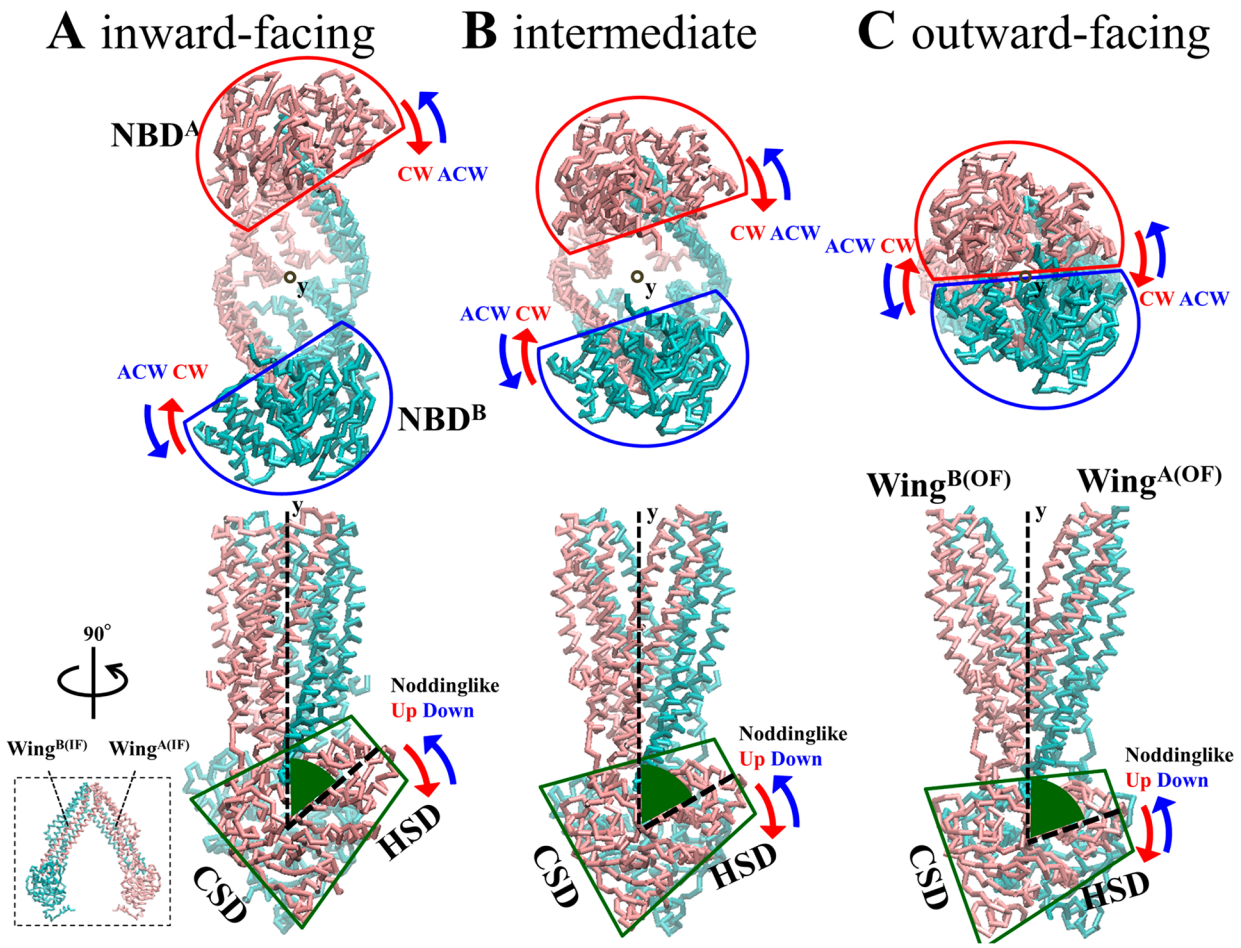

Figure 8. Relationships between the NBD−TMD reverse-rotational and noddinglike motions and the structural change between the inward- and outward-facing states. The inward-facing, intermediate, and outward-facing conformations are represented by backbones in panel A−C, respectively. Chains A and B are colored pink and cyan, respectively. The NBD−TMD reverse-rotational and noddinglike motions during the structural change from the inward- to outward-facing conformation are represented by red arrows, and the corresponding motions from the outward- to inward-facing conformation are indicated by blue arrows. A small view of the 90°-rotated inward-facing conformation is also illustrated in the dotted square at the bottom left.

histidine with alanine results in a loss of ATPase activity.[69] As described above, the MD simulations performed in this study indicate that the interaction between the γ-phosphate of ATP and His357 is weakened by the CH2 mutation. This finding may account for not only the decrease in K_m but also the decrease in k_{cat} by the CH2 mutation.

Role of CHs in the Structure and Dynamics of the ABC Exporters. First, we summarize the features of the dynamics of Wt. In the apo state, the two wings of TMDs were found to approach each other with an increase in the simulation time (Figure 4C), and a synchronous asymmetric NBD opening motion was observed (Figure 5D). It is thus likely that the protein tends to move toward the inward-facing state when found in its apo state. The binding of ATP molecules to the ABPs, however, halts this TMD closing motion and causes the TMDs to move toward a more opened conformation. Simultaneously, the asymmetric motion of the NBDs disappeared. These findings suggest that the outward-facing conformation is stabilized through the binding of ATP. These observations are consistent with those of previous MD studies on the outward-facing state of other exporters, including Sav1866.[27,28,66]

Next, we discuss the effect of the CH mutations that were newly revealed by this study. In the apo state, the asymmetric motion of the NBDs disappeared with the CH2 mutation. Simultaneously, the closing motion of the TMD wings became remarkable compared with those observed for Wt-apo and Mt1-apo (Figure 4C). More importantly, the CH2 mutation generates a similar TMD closing motion even in the ATP-bound state (Figure 4B). According to the PCA results, the CH2 mutant (Mt2-ATP) exhibits an anticlockwise (ACW) rotation, which corresponds to a motion that would result in a structural change from the outward- to inward-facing states as discussed below. These findings imply that CH2 plays a role in the maintenance of the extracellular side of TMDs in the open state while the NBDs are dimerized. Taken together, the data demonstrate that CH2 is a key structural element that mechanically supports the outward-facing conformation and mediates the allosteric communication between the NBDs and TMDs. This is consistent with our experimental finding that the CH2 mutation exerts a stronger influence on the ATPase activity than does the CH1 mutation.

It is of great interest to understand how the NBD−TMD reverse-rotational motion found in our collective motion analysis contributes to the conformational transition between the inward- and outward-facing states. For this purpose, the inward-facing (PDB entry 3B5W[20]) and outward-facing (PDB entry 3B60[20]) conformations were submitted to the morphing

dx.doi.org/10.1021/bi500255j | Biochemistry 2014, 53, 4261−4272

module (g_morph) in the GROMACS program package,[47] and several intermediate structures were created through linear interpolation. One of the resulting morphing conformations (Figure 8B) shows that during the conformational change from the inward- to outward-facing state, each NBD undergoes a CW rotation about the *y*-axis, which passes its center of mass (Figure 8, top). Concomitantly, the orientation of HSD relative to the molecular axis is changed in an upward manner (red arrow in Figure 8) because CH2 pushes the HSD (see Figure 7D). Conversely, in the transition from the outward- to inward-facing state, each NBD exhibits an ACW rotation and HSD undergoes a downward motion (blue arrows in Figure 8). These upward and downward motions of the HSD that are induced by CH2 lead to the generation of a noddinglike motion by the NBDs relative to the TMDs. Therefore, the combined dynamics of the reverse rotation with the noddinglike motion between NBDs and TMDs is indispensable for the conformational transition between the inward- and outward-facing conformations. The movies of these reverse-rotation and noddinglike motions are given in the Supporting Information (Movies M1 and M2). This finding is supported by a recent report by Loo et al., who found that the locking of CHs at one NBD through the cross-linking of cysteines inactivates the human P-glycoprotein.[70]

It is well-known that the ABC "exporters" include two coupling helices (CH1 and CH2) in their 3D structures, whereas only one coupling helix (abbreviated CH_{im}) is found in ABC importers, such as bacterial maltose transporter $MalFGK_2$-E[71−73] and bacterial vitamin B_{12} transporter BtuCD-F.[74−76] This CH_{im} is crucial for the function of ABC importers;[77] the CH_{im} is also called the "EAA" motif because it is highly conserved in all of the small and large importers. From a structural point of view, CH_{im} is embedded in the grooves at the boundary of the RecA-like CSD and HSD, even though it interacts with the same subunit NBD and is not swapped. Judging from its location in the protein, CH_{im} corresponds to CH2 rather than CH1 in ABC exporters. As a result, the more functionally important CH is likely conserved in the ABC importers.

In conclusion, CH2 is significantly important for the maintenance of good ATPase activity in the resulting protein and for the structural transition between the inward- and outward-facing conformations, and both CH1 and CH2 contribute to ATP binding. These findings provide important insights into the structure−function relationship of ABC transporters.

■ ASSOCIATED CONTENT

Supporting Information

Seven conserved motifs in ABPs (Figure S1), the position of the coupling helices (CH1 and CH2) on the RecA-like CSD and HSD (Figure S2), the rmsds for the whole protein in the MD simulations (Figure S3), the interterminal distances on the extracellular side ($Met276^A$−$Met276^B$) (Figure S4), plots of the interactions of ATP with the H-loop in the ATP-bound state (Figure S5), the contribution of each PC for Wt-ATP, Mt1-ATP, and Mt2-ATP systems (Figure S6), the results of PCA of the initial phases in the ATP-bound state for three runs using GROMOS-87 with corrections and for those using GROMOS43A1-S3 (Figure S7), the results of PCA of the whole periods in the apo state (Figure S8), the results of interacting residues of CH1 and CH2 (Table S1), and the reverse-rotation and noddinglike motions (Movies M1 and M2, respectively). This material is available free of charge via the Internet at http://pubs.acs.org.

■ AUTHOR INFORMATION

Corresponding Author

*Telephone: +81-45-924-5795. Fax: +81-45-924-5795. E-mail: msakurai@bio.titech.ac.jp.

Funding

This work was supported by Grants-in-Aid for Scientific Research on Innovative Areas 20118006 and 26104511 (to M.S.) and 23118709 (to H.K.) and for Scientific Research for Young Scientists (B) 25870220 (to T.F.) from the Ministry of Education, Culture, Sports, Science and Technology of Japan.

Notes

The authors declare no competing financial interest.

■ REFERENCES

(1) Holland, I. B., Cole, S. P. C., Kuchler, K., and Higgins, C. F. (2002) *ABC Proteins: From Bacteria to Man*, Academic Press, Amsterdam.

(2) Linton, K. J. (2007) Structure and function of ABC transporters. *Physiology 22*, 122−130.

(3) Rees, D. C., Johnson, E., and Lewinson, O. (2009) ABC transporters: The power to change. *Nat. Rev. Mol. Cell Biol. 10*, 218−227.

(4) Dassa, E., and Bouige, P. (2001) The ABC of ABCs: A phylogenetic and functional classification of ABC systems in living organisms. *Res. Microbiol. 152*, 211−229.

(5) Moussatova, A., Kandt, C., O'Mara, M. L., and Tieleman, D. P. (2008) ATP-binding cassette transporters in *Escherichia coli*. *Biochim. Biophys. Acta 1778*, 1757−1771.

(6) Gottesman, M. M., Fojo, T., and Bates, S. E. (2002) Multidrug resistance in cancer: Role of ATP-dependent transporters. *Nat. Rev. Cancer 2*, 48−58.

(7) Sharom, F. J. (1997) The P-glycoprotein efflux pump: How does it transport drugs? *J. Membr. Biol. 160*, 161−175.

(8) Borges-Walmsley, M. I., McKeegan, K. S., and Walmsley, A. R. (2003) Structure and function of efflux pumps that confer resistance to drugs. *Biochem. J. 376*, 313−338.

(9) Walker, J. E., Saraste, M., Runswick, M. J., and Gay, N. J. (1982) Distantly related sequences in the α- and β-subunits of ATP synthase, myosin, kinases and other ATP-requiring enzymes and a common nucleotide binding fold. *EMBO J. 1*, 945−951.

(10) Schmitt, L., and Tampé, R. (2002) Structure and mechanism of ABC transporters. *Curr. Opin. Struct. Biol. 12*, 754−760.

(11) Ambudkar, S. V., Kim, I.-W., Xia, D., and Sauna, Z. E. (2006) The A-loop, a novel conserved aromatic acid subdomain upstream of the Walker A motif in ABC transporters, is critical for ATP binding. *FEBS Lett. 580*, 1049−1055.

(12) Hung, L.-W., Wang, I. X., Nikaido, K., Liu, P.-Q., Ames, G. F.-L., and Kim, S.-H. (1998) Crystal structure of the ATP-binding subunit of an ABC transporter. *Nature 396*, 703−707.

(13) Smith, P. C., Karpowich, N., Millen, L., Moody, J. E., Rosen, J., Thomas, P. J., and Hunt, J. F. (2002) ATP binding to the motor domain from an ABC transporter drives formation of a nucleotide sandwich dimer. *Mol. Cell 10*, 139−149.

(14) Chen, J., Lu, G., Lin, J., Davidson, A. L., and Quiocho, F. A. (2003) A tweezers-like motion of the ATP-binding cassette dimer in an ABC transport cycle. *Mol. Cell 12*, 651−661.

(15) Schmitt, L., Benabdelhak, H., Blight, M. A., Holland, I. B., and Stubbs, M. T. (2003) Crystal structure of the nucleotide-binding domain of the ABC-transporter haemolysin B: Identification of a variable region within ABC helical domains. *J. Mol. Biol. 330*, 333−342.

(16) Verdon, G., Albers, S.-V., van Oosterwijk, N., Dijkstra, B. W., Driessen, A. J. M., and Thunnissen, A.-M. W. H. (2003) Formation of the productive ATP-Mg^{2+}-bound dimer of GlcV, an ABC-ATPase from *Sulfolobus solfataricus*. *J. Mol. Biol. 334*, 255−267.

(17) Zaitseva, J., Jenewein, S., Jumpertz, T., Holland, I. B., and Schmitt, L. (2005) H662 is the linchpin of ATP hydrolysis in the nucleotide-binding domain of the ABC transporter HlyB. *EMBO J. 24*, 1901−1910.
(18) Dawson, R. J. P., and Locher, K. P. (2006) Structure of a bacterial multidrug ABC transporter. *Nature 443*, 180−185.
(19) Dawson, R. J. P., and Locher, K. P. (2007) Structure of the multidrug ABC transporter Sav1866 from *Staphylococcus aureus* in complex with AMP-PNP. *FEBS Lett. 581*, 935−938.
(20) Ward, A., Reyes, C. L., Yu, J., Roth, C. B., and Chang, G. (2007) Flexibility in the ABC transporter MsbA: Alternating access with a twist. *Proc. Natl. Acad. Sci. U.S.A. 104*, 19005−19010.
(21) Hollenstein, K., Dawson, R. J. P., and Locher, K. P. (2007) Structure and mechanism of ABC transporter proteins. *Curr. Opin. Struct. Biol. 17*, 412−418.
(22) Oancea, G., O'Mara, M. L., Bennett, W. F. D., Tieleman, D. P., Abele, R., and Tampé, R. (2009) Structural arrangement of the transmission interface in the antigen ABC transport complex TAP. *Proc. Natl. Acad. Sci. U.S.A. 106*, 5551−5556.
(23) Bobadilla, J. L., Macek, M., Fine, J. P., and Farrell, P. M. (2002) Cystic fibrosis: A worldwide analysis of CFTR mutations—correlation with incidence data and application to screening. *Hum. Mutat. 19*, 575−606.
(24) Guggino, W. B., and Stanton, B. A. (2006) New insights into cystic fibrosis: Molecular switches that regulate CFTR. *Nat. Rev. Mol. Cell Biol. 7*, 426−436.
(25) Riordan, J. R. (2005) Assembly of functional CFTR chloride channels. *Annu. Rev. Physiol. 67*, 701−718.
(26) Loo, T. W., Bartlett, M. C., and Clarke, D. M. (2013) Human P-glycoprotein Contains a Greasy Ball-and-Socket Joint at the Second Transmission Interface. *J. Biol. Chem. 288*, 20326−20333.
(27) Aittoniemi, J., de Wet, H., Ashcroft, F. M., and Sansom, M. S. P. (2010) Asymmetric switching in a homodimeric ABC transporter: A simulation study. *PLoS Comput. Biol. 6*, e1000762.
(28) Oliveira, A. S., Baptista, A. M., and Soares, C. M. (2011) Conformational changes induced by ATP-hydrolysis in an ABC transporter: A molecular dynamics study of the Sav1866 exporter. *Proteins: Struct., Funct., Bioinf. 79*, 1977−1990.
(29) Gyimesi, G., Ramachandran, S., Kota, P., Dokholyan, N. V., Sarkadi, B., and Hegedűs, T. (2011) ATP hydrolysis at one of the two sites in ABC transporters initiates transport related conformational transitions. *Biochim. Biophys. Acta 1808*, 2954−2964.
(30) Jones, P. M., and George, A. M. (2012) Role of the D-loops in allosteric control of ATP hydrolysis in an ABC transporter. *J. Phys. Chem. A 116*, 3004−3013.
(31) Wise, J. G. (2012) Catalytic transitions in the human MDR1 P-glycoprotein drug binding sites. *Biochemistry 51*, 5125−5141.
(32) Oliveira, A. S. F., Baptista, A. M., and Soares, C. M. (2011) Inter-domain communication mechanisms in an ABC importer: A molecular dynamics study of the MalFGK$_2$E complex. *PLoS Comput. Biol. 7*, e1002128.
(33) Terakado, K., Kodan, A., Nakano, H., Kimura, Y., Ueda, K., Nakatsu, T., and Kato, H. (2010) Deleting two C-terminal α-helices is effective to crystallize the bacterial ABC transporter *Escherichia coli* MsbA complexed with AMP-PNP. *Acta Crystallogr. D66*, 319−323.
(34) Weng, J.-W., Fan, K.-N., and Wang, W.-N. (2010) The conformational transition pathway of ATP binding cassette transporter MsbA revealed by atomistic simulations. *J. Biol. Chem. 285*, 3053−3063.
(35) Ward, A. B., Guvench, O., and Hills, R. D. (2012) Coarse grain lipid−protein molecular interactions and diffusion with MsbA flippase. *Proteins: Struct., Funct., Bioinf. 80*, 2178−2190.
(36) Borbat, P. P., Surendhran, K., Bortolus, M., Zou, P., Freed, J. H., and McHaourab, H. S. (2007) Conformational motion of the ABC transporter MsbA induced by ATP hydrolysis. *PLoS Biol. 5*, e271.
(37) Dong, J., Yang, G., and Mchaourab, H. S. (2005) Structural basis of energy transduction in the transport cycle of MsbA. *Science 308*, 1023−1028.
(38) Woebking, B., Reuter, G., Shilling, R. A., Velamakanni, S., Shahi, S., Venter, H., Balakrishnan, L., and van Veen, H. W. (2005) Drug-lipid A interactions on the *Escherichia coli* ABC transporter MsbA. *J. Bacteriol. 187*, 6363−6369.
(39) Buchaklian, A. H., and Klug, C. S. (2006) Characterization of the LSGGQ and H motifs from the *Escherichia coli* lipid A transporter MsbA. *Biochemistry 45*, 12539−12546.
(40) Westfahl, K. M., Merten, J. A., Buchaklian, A. H., and Klug, C. S. (2008) Functionally important ATP binding and hydrolysis sites in *Escherichia coli* MsbA. *Biochemistry 47*, 13878−13886.
(41) Doshi, R., Woebking, B., and van Veen, H. W. (2010) Dissection of the conformational cycle of the multidrug/lipid A ABC exporter MsbA. *Proteins: Struct., Funct., Bioinf. 78*, 2867−2872.
(42) Syberg, F., Suveyzdis, Y., Kötting, C., Gerwert, K., and Hofmann, E. (2012) Time-resolved Fourier transform infrared spectroscopy of the nucleotide-binding domain from the ATP-binding cassette transporter MsbA: ATP hydrolysis is the rate-limiting step in the catalytic cycle. *J. Biol. Chem. 287*, 23923−23931.
(43) Doshi, R., Ali, A., Shi, W., Freeman, E. V., Fagg, L. A., and van Veen, H. W. (2013) Molecular Disruption of the Power Stroke in the ATP-binding Cassette Transport Protein MsbA. *J. Biol. Chem. 288*, 6801−6813.
(44) Chifflet, S., Torriglia, A., Chiesa, R., and Tolosa, S. (1988) A method for the determination of inorganic phosphate in the presence of labile organic phosphate and high concentrations of protein: Application to lens ATPases. *Anal. Biochem. 168*, 1−4.
(45) Lomize, M. A., Lomize, A. L., Pogozheva, I. D., and Mosberg, H. I. (2006) OPM: Orientations of proteins in membranes database. *Bioinformatics 22*, 623−625.
(46) Kandt, C., Ash, W. L., and Peter Tieleman, D. (2007) Setting up and running molecular dynamics simulations of membrane proteins. *Methods 41*, 475−488.
(47) van der Spoel, D., Lindahl, E., Hess, B., Groenhof, G., Mark, A. E., and Berendsen, H. J. C. (2005) GROMACS: Fast, flexible, and free. *J. Comput. Chem. 26*, 1701−1718.
(48) van Gunsteren, W. F., and Berendsen, H. J. C. (1987) *Groningen Molecular Simulation (GROMOS) Library Manual*, Biomos B. V. Nijenborgh, Groningen, The Netherlands.
(49) van Buuren, A. R., Marrink, S. J., and Berendsen, H. J. C. (1993) A molecular dynamics study of the decane/water interface. *J. Phys. Chem. 97*, 9206−9212.
(50) Mark, A. E., van Helden, S. P., Smith, P. E., Janssen, L. H. M., and van Gunsteren, W. F. (1994) Convergence Properties of Free Energy Calculations: α-Cyclodextrin Complexes as a Case Study. *J. Am. Chem. Soc. 116*, 6293−6302.
(51) Berendsen, H. J. C., Postma, J. P. M., van Gunsteren, W. F., and Hermans, J. (1981) Interaction models for water in relation to protein hydration. In *Intermolecular Forces* (Pullman, B., Ed.) pp 331−342, D. Reidel Publishing Co., Dordrecht, The Netherlands.
(52) Berger, O., Edholm, O., and Jähnig, F. (1997) Molecular dynamics simulations of a fluid bilayer of dipalmitoylphosphatidylcholine at full hydration, constant pressure, and constant temperature. *Biophys. J. 72*, 2002−2013.
(53) Tieleman, D. P., and Berendsen, H. J. C. (1998) A molecular dynamics study of the pores formed by *Escherichia coli* OmpF porin in a fully hydrated palmitoyloleoylphosphatidylcholine bilayer. *Biophys. J. 74*, 2786−2801.
(54) Nosé, S. (1984) A molecular dynamics method for simulations in the canonical ensemble. *Mol. Phys. 52*, 255−268.
(55) Hoover, W. G. (1985) Canonical dynamics: Equilibrium phase-space distributions. *Phys. Rev. A 31*, 1695−1697.
(56) Parrinello, M., and Rahman, A. (1981) Polymorphic transitions in single crystals: A new molecular dynamics method. *J. Appl. Phys. 52*, 7182−7190.
(57) Darden, T., York, D., and Pedersen, L. (1993) Particle mesh Ewald: An N·log(N) method for Ewald sums in large systems. *J. Chem. Phys. 98*, 10089−10092.

(58) Essmann, U., Perera, L., Berkowitz, M. L., Darden, T., Lee, H., and Pedersen, L. G. (1995) A smooth particle mesh Ewald method. *J. Chem. Phys. 103*, 8577−8593.
(59) Hess, B., Bekker, H., Berendsen, H. J. C., and Fraaije, J. G. E. M. (1997) LINCS: A linear constraint solver for molecular simulations. *J. Comput. Chem. 18*, 1463−1472.
(60) Hess-Coelho, T. A. (2006) A redundant parallel spherical mechanism for robotic wrist applications. *Journal of Mechanical Design 129*, 891−895.
(61) Miyamoto, S., and Kollman, P. A. (1992) Settle: An analytical version of the SHAKE and RATTLE algorithm for rigid water models. *J. Comput. Chem. 13*, 952−962.
(62) Chiu, S.-W., Pandit, S. A., Scott, H. L., and Jakobsson, E. (2009) An Improved United Atom Force Field for Simulation of Mixed Lipid Bilayers. *J. Phys. Chem. B 113*, 2748−2763.
(63) Pandit, S. A., Chiu, S.-W., Jakobsson, E., Grama, A., and Scott, H. L. (2007) Cholesterol Surrogates: A Comparison of Cholesterol and 16:0 Ceramide in POPC Bilayers. *Biophys. J. 92*, 920−927.
(64) Csanády, L. (2010) Degenerate ABC composite site is stably glued together by trapped ATP. *J. Gen. Physiol. 135*, 395−398.
(65) Becker, J.-P., Van Bambeke, F. O., Tulkens, P. M., and Prévos, M. (2010) Dynamics and structural changes induced by ATP binding in Sav1866, a bacterial ABC exporter. *J. Phys. Chem. B 114*, 15948−15957.
(66) Jones, P. M., and George, A. M. (2011) Molecular-dynamics simulations of the ATP/apo state of a multidrug ATP-binding cassette transporter provide a structural and mechanistic basis for the asymmetric occluded state. *Biophys. J. 100*, 3025−3034.
(67) Jones, P. M., and George, A. M. (2002) Mechanism of ABC transporters: A molecular dynamics simulation of a well characterized nucleotide-binding subunit. *Proc. Natl. Acad. Sci. U.S.A. 99*, 12639−12644.
(68) Zhou, Y., Ojeda-May, P., and Pu, J. (2013) H-loop histidine catalyzes ATP hydrolysis in the *E. coli* ABC-transporter HlyB. *Phys. Chem. Chem. Phys. 15*, 15811−15815.
(69) Ernst, R., Kueppers, P., Klein, C. M., Schwarzmueller, T., Kuchler, K., and Schmitt, L. (2008) A mutation of the H-loop selectively affects rhodamine transport by the yeast multidrug ABC transporter Pdr5. *Proc. Natl. Acad. Sci. U.S.A. 105*, 5069−5074.
(70) Loo, T. W., and Clarke, D. M. (2014) Locking Intracellular Helices 2 and 3 Together Inactivates Human P-glycoprotein. *J. Biol. Chem. 289*, 229−236.
(71) Khare, D., Oldham, M. L., Orelle, C., Davidson, A. L., and Chen, J. (2009) Alternating access in maltose transporter mediated by rigid-body rotations. *Mol. Cell 33*, 528−536.
(72) Oldham, M. L., and Chen, J. (2011) Crystal structure of the maltose transporter in a pretranslocation intermediate state. *Science 332*, 1202−1205.
(73) Oldham, M. L., and Chen, J. (2011) Snapshots of the maltose transporter during ATP hydrolysis. *Proc. Natl. Acad. Sci. U.S.A. 108*, 15152−15156.
(74) Locher, K. P., Lee, A. T., and Rees, D. C. (2002) The *E. coli* BtuCD structure: A framework for ABC transporter architecture and mechanism. *Science 296*, 1091−1098.
(75) Hvorup, R. N., Goetz, B. A., Niederer, M., Hollenstein, K., Perozo, E., and Locher, K. P. (2007) Asymmetry in the structure of the ABC transporter-binding protein complex BtuCD-BtuF. *Science 317*, 1387−1390.
(76) Korkhov, V. M., Mireku, S. A., and Locher, K. P. (2012) Structure of AMP-PNP-bound vitamin B12 transporter BtuCD-F. *Nature 490*, 367−372.
(77) Daus, M. L., Grote, M., Müller, P., Doebber, M., Herrmann, A., Steinhoff, H.-J., Dassa, E., and Schneider, E. (2007) ATP-driven MalK Dimer Closure and Reopening and Conformational Changes of the "EAA" Motifs Are Crucial for Function of the Maltose ATP-binding Cassette Transporter (MalFGK2). *J. Biol. Chem. 282*, 22387−22396.